Active control on lateral aerodynamic forces of a full-scale high-speed train under crosswind by steady blowing at the head

Guoming Deng
College of Urban Transportation and Logistics
Shenzhen Technology University
Shenzhen 518118, China
dengguoming@outlook.com

Wenlong Zhao
School of Mechanical Engineering
Shanghai Jiao Tong University
Shanghai 200240, China
zwl123@sjtu.edu.cn

Zhengwei Ma
College of Urban Transportation and Logistics
Shenzhen Technology University
Shenzhen 518118, China
mazhengwei@sztu.edu.cn

Yu Zhou
College of Engineering
Eastern Institute of Technology
Ningbo 315000, China
yuzhou@eitech.edu.cn

Xiongshi Wang
College of Urban Transportation and Logistics
Shenzhen Technology University
Shenzhen 518118, China
wangxiongshi@sztu.edu.cn

ABSTRACT

This study addresses the safety risks posed by crosswind-induced lateral forces on high-speed trains (HSTs) by developing an active flow control strategy using steady blowing. A modified Bayesian optimization framework, integrating CFD convergence criteria to mitigate numerical divergence, was employed to optimize 16 control parameters across eight slot-type actuators at the head of the train. Reynolds-averaged Navier-Stokes equations closed with the *k*-*ω* SST (shear stress transport) turbulence model were validated by experimental data and employed for simulations. Results demonstrate strong nonlinearity in control effectiveness concerning blowing ratio and injection angle. Comparative analysis of cost functions reveals critical trade-offs: optimizing solely for overturning moment achieved a 10.6% reduction but increased drag by 13.1%, whereas a multi-objective approach balancing lateral force, overturning moment, lift, drag, and energy consumption yielded a comparable reduction in overturning moment (9.3%) with only a 1.6% drag penalty. This work validates the necessity of multi-objective optimization for balancing aerodynamic performance and energy efficiency.

INTRODUCTION

Crosswinds cause distinct flow structures on the windward and leeward sides of a high-speed train (HST), which results in lateral force and overturning moment that pose a severe risk to operational safety of the HST. Train overturning accidents caused by crosswinds have been reported over all the world. The Chinese government is planning to raise the speed of HST up to 400 km/h or even 600 km/h. Its aerodynamic forces increase dramatically under crosswinds. For example, the lateral force of the leading or head car of a three-carriage HST at about 200 km/h under a crosswind of 15 m/s accounts for more than 50% of its total lateral force (Niu et al., 2017). Passive measurements such as shape optimization and wind barrier are limited in improving crosswind stability due to the space constraints. Advanced and efficient control techniques are urgently needed. The active flow control (AFC) does not change the shape, which is flexible and less costly. The AFC has achieved substantial aerodynamic drag reductions in the flow control of automobile models and HST (Zhou and Zhang, 2021; Deng et al., 2024a; Xi et al., 2024), which shows great potential to improve the aerodynamic safety of HST. Currently, preliminary studies have been reported in literature on the use of AFC to reduce the lateral aerodynamic forces on HST under crosswinds (Chen et al., 2024; Guo et al., 2024), but combined control of multiple variables has not yet been investigated. Therefore, this study explores more effective blowing control positions and parameters for reducing lateral aerodynamic forces of a full-scale HST, and primarily, a global optimization method based on Bayesian optimization is employed to search for the optimal control schemes.

METHODS

Numerical method and setup

The RANS (Reynolds-averaged Navier-Stokes) equations closed with the *k*-*ω* SST (shear stress transport) turbulence model, which was developed by Menter (1994) from the standard *k*-*ε* equations and the *k*-*ω* equations, were used for simulation. The turbulence model has been demonstrated effective in the flow simulation of HST (Deng et al., 2024b; Xi et al., 2024). An idealized train model and its wind tunnel experiment data under crosswinds (Copley, 1987; Chiu and Squire, 1992) were used to verify the reliability of the simulation method. The train model has a length of about 10.5D, where D = 0.125 m is the cross-section diameter of the cylindrical body, and the nose cross section is given by a semi-elliptical profile, as shown in Fig. 1(a, b).

The pressure coefficient is calculated by $C_p = (p - p_\infty) / (0.5\rho U_\infty^2)$, where ρ is the air density and U_∞ is the freestream velocity. A comparison between the measured and simulated C_p at the four cross-sections of the train is shown in Fig. 1(c-f), exhibiting a good agreement.

A full-scale three-carriage HST model is used, with a length (L), width (W), and height (H) of about 80.65 m, 3.35 m, and 4.03 m, respectively. The train model can be referred to Deng et al. (2024b). To reduce the lateral force and overturning moment, eight slot-type blowing jets are arranged on the leeward side of the train head, shown in Fig. 2(a). The length and width of the eight slots are given in Table 1. The blowing ratio and blowing angle of each slot were varied, and the aforementioned simulation method was employed to solve the flow field around the HST under respective control conditions, followed by calculations of the lateral force and overturning moment.

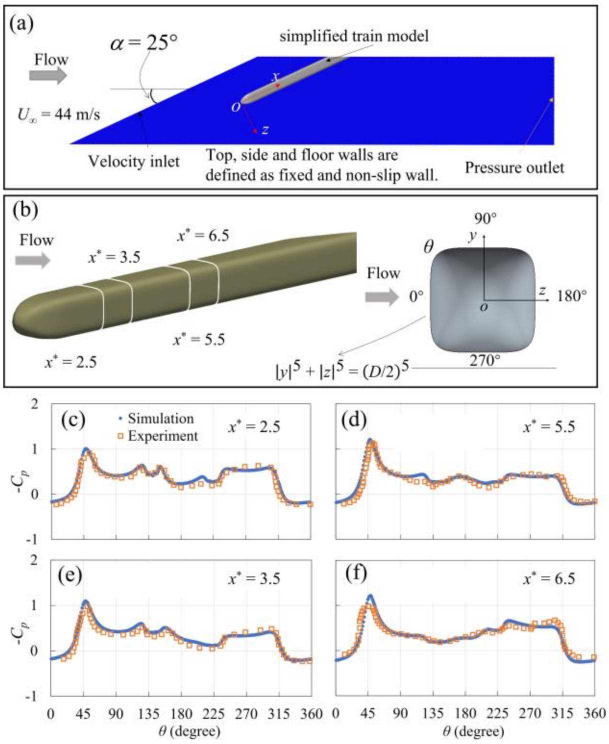

Figure 1. (a) The computation domain, boundary conditions and the geometry of the idealized HST model (Copley, 1987). (b) The details of the geometry and the definition of angular coordinate of the cross-section. (c-f) A comparison of the pressure coefficient at the fore cross sections between the simulation and experiment.

Table 1. Best control results of individual actuations on lateral force coefficient (C_S) and overturning moment coefficient (C_M).

Actuation	Length (m)	Width (m)	Best ΔC_S (%)	Best ΔC_M (%)
S1	2.28	0.030	-3.2	-2.2
S2	3.30	0.030	-2.5	-2.9
S3	2.19	0.050	-3.8	-4.4
S4	0.60	0.020	-2.7	-1.7
S5	0.52	0.025	-2.7	-1.6
S6	0.93	0.030	-3.4	-1.2
S7	1.38	0.028	-4.6	-2.4
S8	1.10	0.028	-3.0	-1.7

The computational domain is discretized using trimmer mesh, as illustrated in Fig. 2(b). Due to the complexity of the wake flow and the near-wall region, the mesh is refined using a tapered cylindrical zone with gradually varying diameters near the train body, and two levels of refinement are applied, including a tapered cylindrical zone and a rectangular zone (Fig 2c). The mesh size decreases progressively closer to the vehicle surface. Prism layer meshes are employed near the walls to simulate the flow within the boundary layer. The total thickness of the prism layers is 0.012 m, consisting of 8 layers with a growth rate of 1.2. The dimensionless wall distance y^+ ($= u_\tau y_w/\nu$, where u_τ is the wall friction velocity and $\nu = 1.51 \times 10^{-5}$ m^2 s^{-1} is the kinematic viscosity of air) at the center of the first layer off the wall is approximately 115, suitable for engineering simulations of full-scale HST (Muñoz-Paniagua and García, 2020; Sun *et al.*, 2021). The surface mesh size at the head, tail, and in wheel-rail or ballast regions of the train is approximately 50 mm, while the mesh size of the slot regions is about 15 mm (Fig. 2d). The mesh size in the straight middle regions and of the ground is approximately 100 mm and 2.5 m, respectively, while the mesh sizes at the inlet, outlet, sides, and top of the computational domain are approximately 4.5 m. The volume mesh in regions far from the train surface is relatively coarse to reduce computational cost.

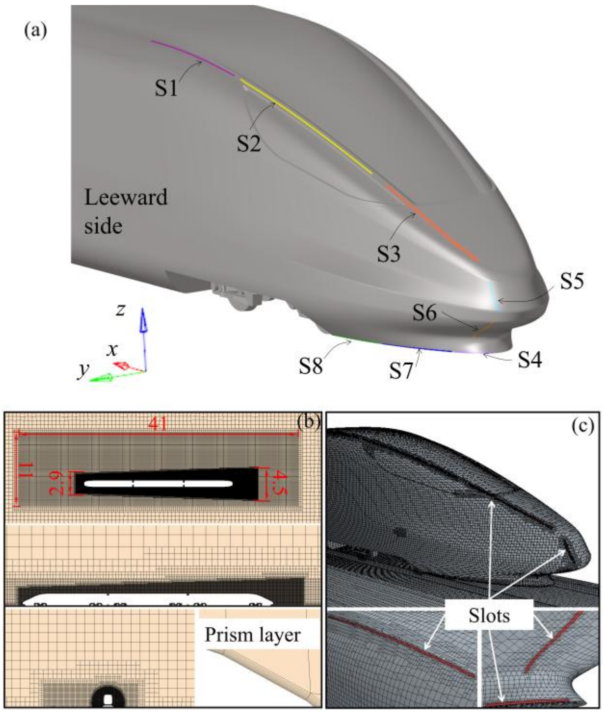

Figure 2. (a) schematic locations of the eight independent slot-type actuations. (b) The mesh around the train body, and prism-layer meshes. (c) Mesh on the train surface and slot surfaces. The dimensions are dimensionless, normalized by $\sqrt{A}$.

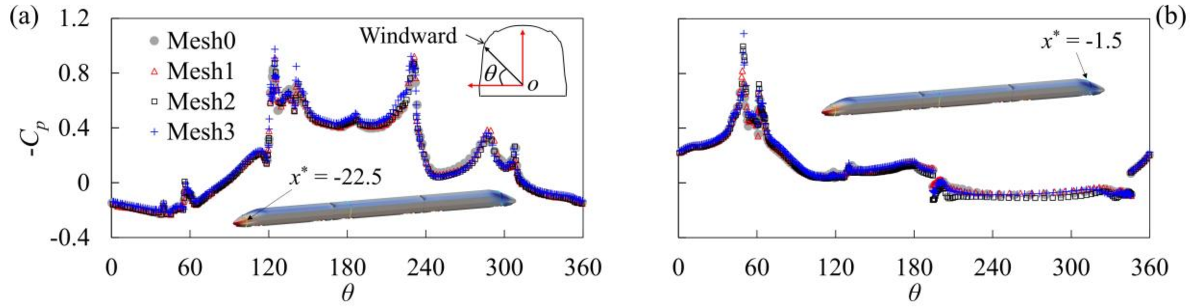

Figure 3. Numerical results obtained from the four mesh schemes: C_p distributions at the cross-sections of x^* = -22.5 (a), and -1.5 (b), respectively.

A grid-independence study was performed using four mesh densities to ensure computational accuracy while minimizing resource consumption in simulating the flow of the full-scale HST model. Angular coordinates are introduced to describe surface locations, which facilitates the comparison of pressure coefficients. The four mesh discretization schemes (Mesh0 – Mesh3) have cell counts of approximately 5.3, 12.8, 19.8, and 32 million, respectively.

The computed C_p distributions are shown in Fig. 3(a-b), with definition of the angular coordinates illustrated in Fig. 3(a). The results from Mesh0 deviate noticeably from those of the three finer meshes (Mesh1 – Mesh3), especially beneath the train body. In contrast, the C_p distribution obtained with Mesh1 agrees closely with the two finer meshes (Mesh2 and Mesh3).

Bayesian optimization

The surrogate-model-based optimization characterized by infill-sampling strategy is used in this work. The pioneer works can be referred to Mockus (1994) and Jones et al. (1998). It begins with a limited number of initial samples of the control variables, which are generated by Latin hypercubic sampling, and their objective or cost functions (aerodynamic forces) evaluated by the simulation method. A Kriging surrogate model is trained by the initial samples. After that, the optimization goes into the iterative process. At each iteration, an acquisition function defined from infill criterion is used as an optimization objective, and searching for the objective generates a new sample point, which could approach the local optima or global optima following the exploitation or exploration of the acquisition function. The new sample point is added into the data set for upgrading the surrogate model, and then the process goes to the next iteration, until a termination condition is satisfied. This study employs a modified Bayesian optimization method to the investigation on crosswind safety control of a full-scale HST.

Active control requires additional energy input. It is evident that a higher blowing velocity demands larger energy supply. Although mitigating crosswind effects to enhance train operational safety is of great importance, we aim to balance the energy consumption with safety enhancement. Therefore, the energy consumption of blowing is evaluated, and the optimization of control parameters aims to enhance safety with minimal energy expenditure. An energy consumption coefficient (C_E) is defined as follows,

$$C_E = \sum_{j=1}^{N} \frac{S_j U_j^3}{A U_\infty^3} = \frac{1}{A} \sum_{j=1}^{N} S_j B_{rj}^3 \tag{1}$$

where N is the number of slots, and S_j and U_j denote the outlet area and blowing velocity of the j-th slot, respectively. The A (= 11.94 m^2) indicates the projected area of the train along the longitudinal direction. The $B_{rj} = U_j / U_\infty$ denotes the blowing ratio of the j-th slot. The C_E is proportional to the cube of the blowing velocity, which is consistent with the energy consumption evaluation metric used in the literature (Chen *et al.*, 2024; Guo *et al.*, 2024a).

Considering the energy consumption coefficient, we design a cost function as follows,

$$J(\boldsymbol{B_r}, \boldsymbol{\gamma}) = \alpha_1 C_D + \alpha_2 C_L + \alpha_3 C_S + \alpha_4 C_M + \alpha_5 C_E \tag{2}$$

where $\boldsymbol{B_r} = [B_{r1}, B_{r2}, \ldots, B_{rN}]^T$ and $\boldsymbol{\gamma} = [\gamma_1, \gamma_2, \ldots, \gamma_N]^T$ are the vectors of blowing ratios and angles, respectively. The γ is defined as following: when perpendicular to the surface, $\gamma = 0$; when deviating toward the y-axis, γ is positive; and when deviating away from the y-axis, the γ is negative. α_1, α_2, α_3, α_4, and α_5 are the weighting coefficients. The aerodynamic force/moment coefficients C_α in this study include the drag coefficient (C_D), the lift coefficient (C_L), the lateral force coefficient [$C_S = F_S$ / $(0.5\rho U_\infty^2 A)$] and overturning moment coefficient [$C_M = M_x$ / $(0.5\rho U_\infty^2 A L_r)$], where the L_r indicates a constant reference length of 3 m. The F_S and M_x denote the lateral force and overturning moment, respectively. The rotation axis for overturning moment calculation is located at the outer side of upper surface of the leeward wheel hub. The freestream velocity for the full-scale HST is U_∞ = 400 km/h. The change in C_α is defined as $\Delta C_\alpha = (F_\alpha - F_{\alpha 0}) / F_{\alpha 0}$, where F_α and $F_{\alpha 0}$ indicate the controlled and uncontrolled force or moment.

To find the optimal cost function value, a surrogate model is employed to establish the functional relationship between the control parameters ($\boldsymbol{B_r}$, $\boldsymbol{\gamma}$) and the cost function J. Optimization algorithms are then used to search for the optimal control parameters. This optimization problem is formulated as follows,

$$\begin{aligned} &\text{Minimize } J(\boldsymbol{B}_r, \boldsymbol{\gamma}) \\ &\text{s.t. } \boldsymbol{B}_{rl} \le \boldsymbol{B}_r \le \boldsymbol{B}_{ru} \text{ and } \boldsymbol{\gamma}_l \le \boldsymbol{\gamma} \le \boldsymbol{\gamma}_u \end{aligned} \tag{3}$$

where $\boldsymbol{B_{rl}}$, $\boldsymbol{\gamma_l}$ and $\boldsymbol{B_{ru}}$, $\boldsymbol{\gamma_u}$ are the lower and upper bounds of the control parameters, respectively. This study uses identical control parameter ranges to all actuators. Specifically, the ranges for $\boldsymbol{B_r}$ and $\boldsymbol{\gamma}$ are [0, 2] and [-85, 85], respectively.

RESULTES AND DISCUSSION

By comparing the lateral aerodynamic forces before and after the implementation of blowing control, the maximum reductions in lateral force and overturning moment achieved under each actuation are summarized in Table 1. Among the eight slots, the S7 achieves the largest reduction in C_S by 4.6% at $(B_r, \gamma) = (0.5, 0°)$, and the S3 yields the largest reduction in C_M by 4.4% at $(B_r, \gamma) = (1.3, -25°)$.

The reduction in C_S and C_M achieved through steady blowing control at the full-scale HST's head is dependent on the blowing location, B_r, and γ. The influence of B_r and γ on the force/moment of the actuations S3 and S7 (Fig. 4) shows strong nonlinearity. It is seen from Fig. 4(a) that, when B_r varies from 0.1 to 1.5, the C_S of S3 increases first, then decreases from 0.3 to 1.1 before going up again. Nonlinear property is also seen from the results of Fig. 4(b-d).

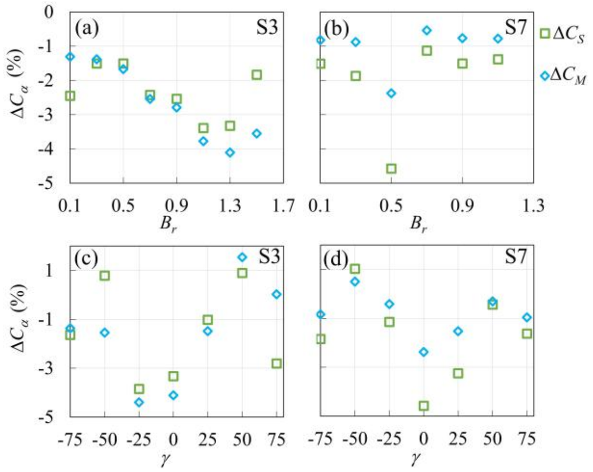

Figure 4. (a, b) Changes of C_S and C_S for actuation S3 and S7 versus the blowing ratio (B_r). (c, d) Changes of C_S and C_S for actuation S3 and S7 versus the blowing angle (γ).

The Impact of CFD Divergence on Optimization

In the preliminary exploratory phase, we attempted three optimization test cases, i.e., Case1, Case2, and Case3 in Table 2. During the Bayesian optimization iterative process, certain control parameters caused the CFD calculations to diverge. In the optimization workflow, the divergent results were included in the training dataset, which prevented the convergence of the overall optimization process, as shown in Fig. 5. This is a result of contamination by anomalous data.

The optimization process was contaminated by abnormal data (CFD divergence), causing the samples added by the surrogate during the Bayesian optimization to be scattered and disordered. Nevertheless, some control schemes were still obtained, though not particularly pronounced. For example, the maximum reduction rates of the overturning moment for Case 1, Case 2, and Case 3 were 6.5%, 6.8%, and 5.5%, respectively.

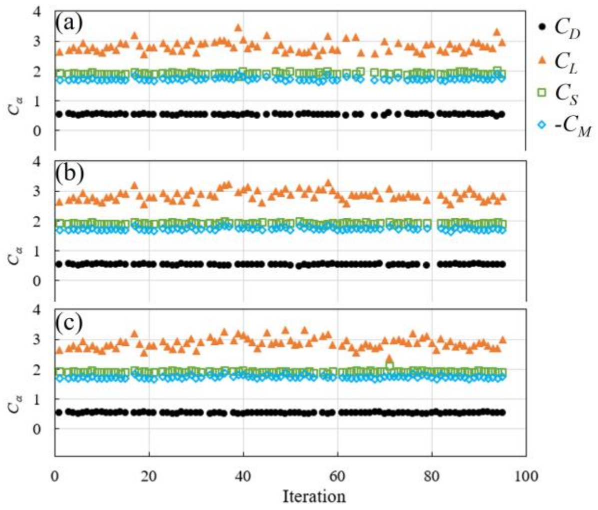

Figure 5. Bayesian optimization process of Case1 (a), Case2 (b) and Case3 (c): Variation of aerodynamic force/moment coefficients with iterations.

Table 2. Case study on combined control optimization of multi-parameter for multi-slot blowing on the leeward side of a full-scale 3-carriage HST using Bayesian optimization.

Case	Weighted coefficients [α_1, α_2, α_3, α_4, α_5]	Infill criterion	Algorithm
Case1	[1.92, 0.336, 0.522, -**0.568**, 0]	LCB	LBFGS
Case2	[1.92, 0.336, 0.522, -**5.68**, 0]	LCB	LBFGS
Case3	[0.017, 0.003, 0.75, -0.05, 0]	LCB	LBFGS
Case4	[0.017, 0.003, 0.75, -0.05, 1]	LCB+EI	LBFGS+GA
Case5	[0, 0, 0, -**0.2865**, **5**]	LCB+EI	LBFGS+GA
Case6	[0, 0, 0, -**0.5672**, 0]	LCB+EI	LBFGS+GA

The impact of weighting coefficients on optimization

To prevent abnormal data from affecting the training of surrogate models, we have incorporated a convergence criterion for CFD simulations. If the CFD solution diverges, we discard the corresponding dataset.

Figure 6 compares the results of the Case 4-5 listed in Table 2. These three schemes share the same infill criterion and optimization algorithm but differ in the weighting coefficients of the cost function. The cost function of Case4 emphasizes all five target performance objectives, with weighting coefficients (α_1, α_2, α_3, α_4, α_5) = (0.017, 0.003, 0.75, -0.05, 1). As shown in Figure

6(a, b), the first 48 samples are from Latin Hypercube Sampling, exhibiting uniform distribution characteristics, while during the optimization process, all coefficients display strong convergence and local exploitation characteristics. After optimization, the maximum reduction rate of C_M is 9.3%, corresponding to C_E = 0.1928, and reduction in J by 7.7%. The cost function of Case5 emphasizes overturning moment and energy consumption coefficient. The optimization process also exhibits local exploitation characteristics, with the maximum overturning moment reduction rate reaching 7.7%, corresponding to C_E = 0.0908, and reduction in J by only 1.7%. The cost function of Case6 considers only the overturning moment. The optimization process shows local exploitation characteristics, achieving a maximum C_M reduction rate of 10.6%, corresponding to C_E = 0.1996, and reduction in J also by 10.6%.

The weighting coefficients in Case4 consider C_D, C_L, C_S, C_M, and C_E simultaneously, whereas Case6 considers only C_M. The results indicate that the maximum reduction in C_M achieved by Case6 is more significant than that of Case4. However, Case6 leads to a 13.1% increase in C_D, compared to a mere 1.6% increase in Case4. In Case5, the cost function assigns a higher weight to C_E; consequently, the optimal C_M corresponds to an C_E value that is only half of those observed in Case4 or Case6 (see Table 3). Moreover, the C_D and C_L are increased in Case5 by 2.8% and 3.6%, respectively, whilst the C_S is reduced by 13.2%.

Table 3. The maximum reduction in C_M and the corresponding C_E and J for the three cases (Case 4-5).

Case	Maximum reduction in C_M (%)	C_E	Reduction in J (%)
Case4	9.3	0.1928	7.7
Case5	7.7	0.0908	1.7
Case6	10.6	0.1996	10.6

CONCLUSIONS

This study demonstrates that the effectiveness of active flow control on mitigating crosswind effects of high-speed trains is highly dependent on slot location, blowing ratio (B_r), and injection angle (γ), exhibiting strong nonlinearity. While initial optimization attempts (Case 1–3) were compromised by CFD divergence, the integration of convergence criteria successfully mitigated this issue. Comparative analysis of the cost function weighting revealed distinct outcomes: Case6, focusing solely on the overturning moment (C_M), achieved the most significant C_M reduction (10.6%) but at the expense of a substantial drag (C_D) increase (13.1%). In contrast, Case4, which balanced multiple objectives (C_D, C_L, C_S, C_M, C_E), yielded a comparable C_M reduction with a negligible C_D penalty (1.6%). Furthermore, prioritizing energy consumption (Case5) resulted in both C_M reduction (7.7%) and lower energy consumption, almost half of that achieved by Case4 or Case6. Therefore, multi-objective

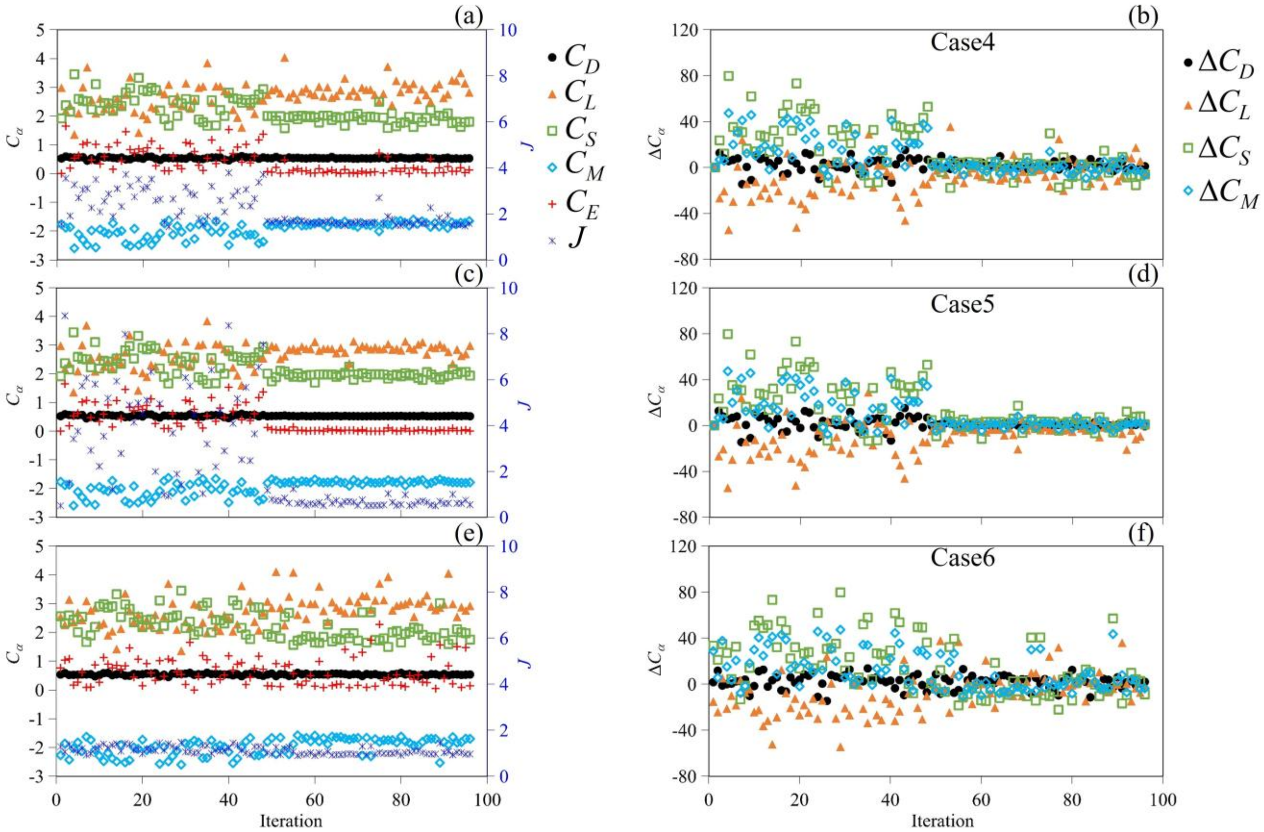

Figure 6. Bayesian optimization process: (Left column) Variation of aerodynamic force/moment coefficients, energy consumption coefficient, and cost function with iterations; (Right column) Variation of the rate of change of aerodynamic force/moment coefficients with iterations. (a, b) Case4, (c, d) Case5, and (e, f) Case6.

optimization is crucial for balancing aerodynamic performance and energy efficiency.

ACKNOWLEDGMENTS

The authors wish to acknowledge financial support from NSFC through grant 12302359 and Natural Science Foundation of Top Talent of SZTU through grant GDRC202541.

REFERENCES

Chen, Z. W., Guo, Z. J., Che, Z. X., Huang, Z. D., Ni, Y. Q., Wang, S. M., Huang, S., Li, Z. W., & Wang, Q. X., 2024, "Evaluation of active leeward side air-blowing layout on the lateral aerodynamic performance of high-speed trains in crosswinds environment: Sustainable and safe operation strategy", *Journal of Wind Engineering and Industrial Aerodynamics*, Vol. 247, pp. 105695.

Chiu, T.W., Squire, L.C., 1992, "An experiment study of the flow over a train in a crosswind at large yaw angles up to 90°", *Journal of Wind Engineering and Industrial Aerodynamics*, Vol. 45, pp. 47-74.

Copley, J.M., 1987, "The three-dimensional flow around railway trains", *Journal of Wind Engineering and Industrial Aerodynamics*, Vol. 26(1), pp. 21-52.

Deng, G.M., Fan, D.W., Zhang, B.F., Zhou, Y., 2024a, "Active control for a low-drag Ahmed vehicle model based on steady blowing", *Physics of Fluids*, Vol. 36(1), pp. 015104.

Deng, G.M., Xi, L.C., Zhou, Z., Liu, H.Y., and Zhou, Y., 2024b, "AI-based shape optimization for drag reduction of a high speed train head/tail", *Fluid-Structure-Sound Interactions and Control, Proceedings of the 6th Symposium on Flu-id-Structure-Sound Interactions and Control (Eds. Daegyoum Kim, Kyung Chun Kim, Yu Zhou, Lixi Huang),* pp. 225-232, Springer Berlin Heidelberg.

Guo, Z. J., Guo, Z. H., Chen, Z. W., Zeng, G. Z., & Xu, J. Q., 2024, "On the active flow control in maglev train safety under crosswinds: Analysis of leeward suction and blowing action", *Physics of Fluids*, Vol. 36(9), pp. 095130.

Jones, D.R., Schonlau, M., Welch, W.J., 1998, "Efficient Global Optimization of Expensive Black-Box Functions", *Journal of Global Optimization*, Vol. 13, pp. 455-492.

Menter, F.R., 1994, "Two-equation eddy-viscosity turbulence models for engineering applications", *AIAA Journal*, Vol. 32(8), pp. 1598-1605.

Mockus, J., 1994, "Application of Bayesian approach to numerical methods of global and stochastic optimization", *Journal of Global Optimization*, Vol. 4, pp. 347-365.

Muñoz-Paniagua, J., García, J., 2020, "Aerodynamic drag optimization of a high-speed train", *Journal of Wind Engineering and Industrial Aerodynamics* 204, 104215.

Niu, J., Zhou, D., Liang, X., 2017, "Numerical investigation of the aerodynamic characteristics of high-speed trains of different lengths under crosswind with or without windbreaks", *Engineering Applications of Computational Fluid Mechanics*, 12(1), 195-215.

Sun, Z.X., Wang, M.Y., Wei, L.Y., Kong, F.B., Yang, G.W., 2021, "Aerodynamic shape optimization of an urban maglev train", *Acta Mechanica Sinica* 37, 954-969.

Xi, L.C., Deng, G.M., Zheng, Z.Y., and Zhou, Y., 2024, "Surrogate-model-based active drag reduction of high speed trains", *Fluid-Structure-Sound Interactions and Control, Proceedings of the 6th Symposium on Flu-id-Structure-Sound Interactions and Control (Eds. Daegyoum Kim, Kyung Chun Kim, Yu Zhou, Lixi Huang),* pp. 267-272, Springer Berlin Heidelberg.

Zhou, Y., and Zhang, B.F., 2021, "Recent advances in wake dynamics and active drag reduction of simple automotive bodies", *Applied Mechanics Reviews*, 73(6), 060801.